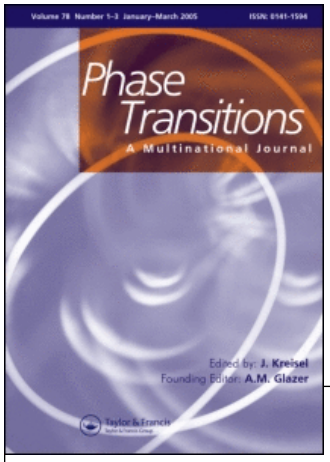

Phase Transitions
A Multinational Journal
Publication details, including instructions for authors and subscription information:
http://www.informaworld.com/smpp/title~content=t713647403

Interface engineering and strain in $YBa_2Cu_3O_{7-\delta}$ thin films

Mark Huijben [a]; Gertjan Koster [a]; Dave H. A. Blank [a]; Guus Rijnders [a]
[a] Faculty of Science and Technology, MESA Institute for Nanotechnology, University of Twente, Enschede, The Netherlands

Online Publication Date: 01 July 2008

To cite this Article: Huijben, Mark, Koster, Gertjan, Blank, Dave H. A. and Rijnders, Guus (2008) 'Interface engineering and strain in $YBa_2Cu_3O_{7-\delta}$ thin films', Phase Transitions, 81:7, 703 — 716

To link to this article: DOI: 10.1080/01411590802063769
URL: http://dx.doi.org/10.1080/01411590802063769

Phase Transitions
Vol. 81, Nos. 7–8, July–August 2008, 703–716

Interface engineering and strain in $YBa_2Cu_3O_{7-\delta}$ thin films

Mark Huijben, Gertjan Koster, Dave H.A. Blank and Guus Rijnders*

Faculty of Science and Technology, MESA Institute for Nanotechnology, University of Twente, Enschede, The Netherlands

(*Received 11 March 2008; final version received 18 March 2008*)

In thin films, new phases can be encountered near interfaces, whether it is the substrate–film interface or subsequent interfaces in the case of heterostructures. Both structural properties and surface morphology are a direct result of the thin film growth, controlled by deposition conditions and substrate properties, which in turn influence the electrical properties and determine their applicability in multilayer structures. At the initial growth stage, the stacking sequence of the individual atomic layers at the interface with the substrate is influenced by the substrate surface properties. During subsequent deposition, the lattice mismatch between substrate and growing film becomes dominant. In this article, an overview is given of the complex growth mechanisms of $YBa_2Cu_3O_{7-\delta}$ on $SrTiO_3$ substrates. The afore mentioned issues will be addressed, with a focus on initial growth, interface engineering and strain, leading to phases that are different from the bulk both structurally and in their superconducting properties.

Keywords: interface engineering; superconductor thin film; strain; thin film growth

1. Introduction

After the discovery of an increased transition temperature in the then new high-T_c $La_{2-x}Sr_xCuO_4$ compound [1], which confirmed the results of the high-pressure experiments on the original $La_{2-x}Ba_xCuO_4$ compound [2,3], attempts were taken in 1987 to shrink the crystal lattice even more. The smaller yttrium was substituted for the lanthanum in the original formula, leading to the discovery of the Y-Ba-Cu-O compound with an increased T_c of 93 K [4]. This was the first time the superconducting state could be obtained beyond the liquid-nitrogen boiling point at 77 K.

The new superconductor was soon identified as $YBa_2Cu_3O_7$ (Y123) [5], with a crystal structure very unlike the structure of any oxide perovskite that had been observed previously, see Figure 1(a). There are two significant differences between this material and the K_2NiF_4-type forerunners. The first is that there are two layers of CuO_2 planes in close proximity (~3.4 Å apart) instead of one. The second is that there are remarkable one-dimensional chains of corner-shared CuO_4 squares running along one of the crystallographic directions. The crystal structure is orthorhombic at room temperature

*Corresponding author. Email: a.j.h.m.rijnders@utwente.nl

ISSN 0141–1594 print/ISSN 1029–0338 online

DOI: 10.1080/01411590802063769
http://www.informaworld.com

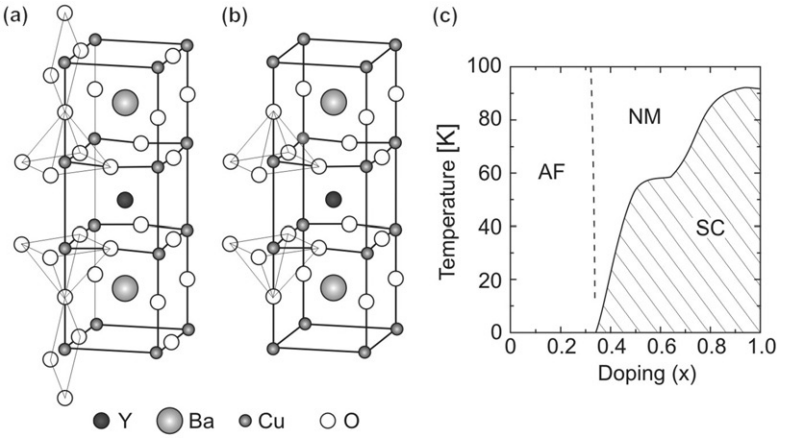

Figure 1. Crystal structures of $YBa_2Cu_3O_7$ (a) and $YBa_2Cu_3O_6$ (b) together with the phase diagram of $YBa_2Cu_3O_{6+x}$ (c) showing magnetic and electronic properties with the dependence on the doping level (x).
Note: Antiferromagnetic (AF), superconducting (SC) and normal metal (NM) regions are indicated.

with a c-axis of $\sim$ 11.7 Å and a- and b-axes of$\sim$3.82 Å and $\sim$3.88 Å. Changes in the oxygen stoichiometry lead to the oxygen deficient $YBa_2Cu_3O_6$, which is nonsuperconducting and tetragonal [6], see Figure 1(b). The dramatic effect of this phase transition on the superconducting properties is shown in Figure 1(c).

Thin film growth of Y123 is, since its discovery, a subject of extensive research and can be achieved by various physical vapor deposition techniques [7]. Independent of the deposition technique, oscillations of the reflection high-energy electron diffraction (RHEED) intensity were observed, caused by two-dimensional layer-by-layer growth [8,9]. It was found that the oscillation period corresponds to the time necessary for the deposition of one unit cell layer in the c-axis direction, which is the growth unit that satisfies charge neutrality. Because of this, a specific stacking sequence of the atomic layers should exist and, the growth unit should always terminate with the same atomic layer. Since the first atomic layer is determined by both substrate and film, the following questions arise:

(1) Is the charge neutral growth unit during the initial, heteroepitaxial growth, i.e., deposition of the first unit cell layer, also the unit cell of Y123 consisting of 6 atomic layers?
(2) Is the terminating atomic layer of the Y123 thin film depending on the terminating atomic layer of the substrate or is it thermodynamically determined by Y123 itself?
(3) Is the terminating atomic layer of the film influenced by the deposition conditions?

Therefore, an important subject for the epitaxial growth of Y123 is the choice of substrate [10], which determines the structural and electrical properties of the fabricated thin films in a nontrivial way.

1.1. *Initial growth at the substrate–film interface*

Perovskite oxides are commonly described in terms of their cubic unit cells, with the generic formula ABO_3. It is instructive to describe the perovskites in terms of their

constituting AO and BO_2 layering sequence. The unit cell of the $SrTiO_3$ (STO) substrate consists of Ti atoms occupying the corner positions and a Sr atom occupying the body center position. The Ti atom is 6-fold coordinated by oxygen, forming the corner-sharing oxygen octahedral. The structure can be viewed as a stack of alternating SrO (AO) and TiO_2 (BO_2) planes along one of the principal axes. The surface of the STO single crystal can, therefore, be terminated by SrO or TiO_2, when cut perpendicular to one of the principal axes, or by a mixture of both. Control of this surface termination can create single-terminated surfaces, which is crucial for accurate growth studies. Single-terminated TiO_2 surfaces are achieved by removing the remaining SrO by a chemical treatment, followed by an annealing procedure [11]. The opposite single-terminated SrO surfaces are fabricated by depositing a SrO monolayer on a single-terminated TiO_2 surface by pulsed laser interval deposition (PliD) [12] from a SrO single-crystal target.

Further, we expect a continuation of the bulk–AO–BO_2–AO perovskite stacking of the substrate and when all constituents are provided simultaneously, for instance, in the case of pulsed laser deposition (PLD), the growth unit is the Y123 unit cell. As mentioned above, one direct implication of this fact is the requirement of a specific stacking sequence of the individual atomic layers constituting this unit-cell. During the initial stage of growth, the stacking sequence will be influenced by the substrate surface properties, i.e., the terminating atomic layer and its crystalline structure. The first atomic layer and, consequently, the sequence of the initial Y123 unit cell layer will depend on these properties. High-resolution electron microscopy (EREM) measurements of the stacking sequence at the interface (SSI) of Y123 on single TiO_2-terminated $SrTiO_3$ (STO) substrates [13] have shown that a perovskite-like interface is present with two SSIs: bulk–SrO–TiO_2–BaO–CuO–BaO–CuO_2–Y–CuO_2–BaO–bulk (referred as Y133) and bulk–SrO–TiO_2–BaO–CuO_2–Y–CuO_2–BaO-bulk (referred as Y122). The coexistence of different SSIs leads to surface roughening and plays an essential role in the formation of antiphase boundaries (APBs) oriented perpendicularly to the substrate-film interface. These APBs, which are the most prominent type of defects occurring in ultrathin Y123 films, start at the interface and persist over the total film thickness. Some authors have related such planar defects to unit-cell steps on the substrate [14,15], but the density of APBs in Y123 ultrathin films grown on TiO_2-terminated STO is large compared to the density of substrate unit cell steps [13], indicating that APBs are formed on the atomically smooth terraces due to the coalescence of neighbouring islands with different SSIs.

2. Experimental

To study the influence of the stacking sequence at the substrate-film interface and the related network of APBs on the electrical properties of *c*-axis oriented Y123 ultrathin films, three different interface configurations are used, see Figure 2.

(1) Y123 on as-received vicinal STO substrates. The surface of these substrates consist of terraces with disordered step ledges and islands on the terraces with height differences of integer numbers of half a unit cell ($\sim$2 Å). This indicates the coexistence of the two possible surface arrangements: SrO- and TiO_2-terminated domains (double-termination (DT)). This will lead to four possible SSIs [16].
(2) Y123 on TiO_2-terminated STO substrates. Using the procedure described in ref. [11], STO substrates are treated in order to get atomically smooth single-terminated TiO_2 surfaces. This will lead to two different SSIs [13].

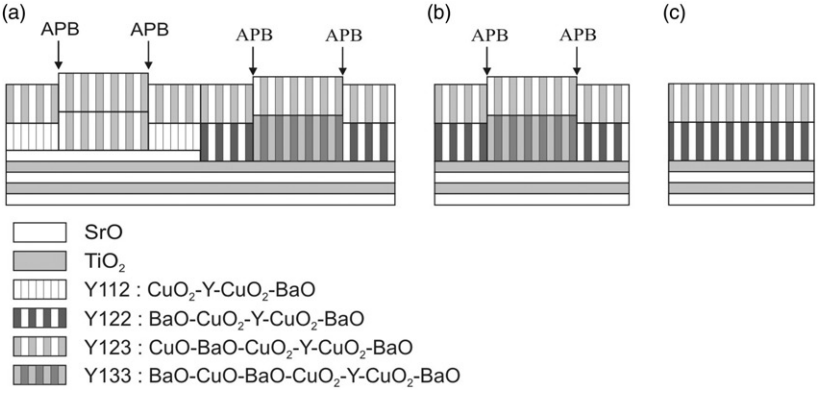

Figure 2. Schematic representation of the three interface configurations used on growing Y123: (a) on as-received DT-STO, where four (SSI) possible, (b) on single TiO_2-terminated STO, allowing two different SSIs, and (c) on TiO_2-terminated STO using Y122 for the first unit cell layer, giving rise to a single SSI.
Notes: In these cases, the coalescence of islands with different stacking sequences causes the formation of APBs, which are indicated by arrows.

(3) Y123/Y122 on TiO_2-terminated STO substrates. Stoichiometric deposition with a cation ratio $Y:Ba:Cu = 1:2:2$ during growth of the first unit-cell layer leads to the precise control of the interface configuration by suppression of the Y133 configuration. This procedure gives rise to only one SSI.

These films, presenting different interface configurations, were deposited by PLD on (100) STO and their growth was *in-situ* monitored by RHEED, allowing control of the thickness. The initial pseudomorphic growth mode changed to island growth to release the epitaxial strain over a critical thickness, which scaled with the inverse of the lattice mismatch. For Y123 on STO, the critical thickness was found to be dependent on the $SrTiO_3$ termination [17] and estimated to be in the range of 20 nm, about 17 u.c., for TiO_2-terminated substrates [18]. All films studied here present thickness ranging from 5 to 10 u.c., which allow study of the influence of the SSI on the superconducting properties without interference from strain relaxation mechanisms.

Concerning the PLD deposition conditions, a sintered ceramic target with the nominal stoichiometry $Y:Ba:Cu = 1:2:3$ was ablated with an energy density of 1.3 J/cm^2 at 1 Hz. During growth, the substrate was held at 780°C in an oxygen environment at 0.13 mbar. Similar temperature and oxygen background pressure conditions were used when depositing the Y122 layer, but the energy density at the target (nominal stoichiometry $Y:Ba:Cu = 1:2:2$) was 7 J cm^{-2}. In this case, (PliD) [12] was used at 50 Hz to obtain an atomically smooth single u.c. layer, followed by *in-situ* annealing for 1 h at 830°C before depositing the Y123 layer. On top of the samples a protective $SrRuO_3$ layer was grown at 600°C in an oxygen pressure of 0.13 mbar to facilitate electrical characterization. Finally, all samples were annealed in an oxygen atmosphere at 0.7 bar for 30 min at, respectively, 600°C and 450°C.

3. Results

In Figure 3, the RHEED specular intensities, recorded during the growth of the Y123 layers with the different interface configurations, are shown. A large recovery of the

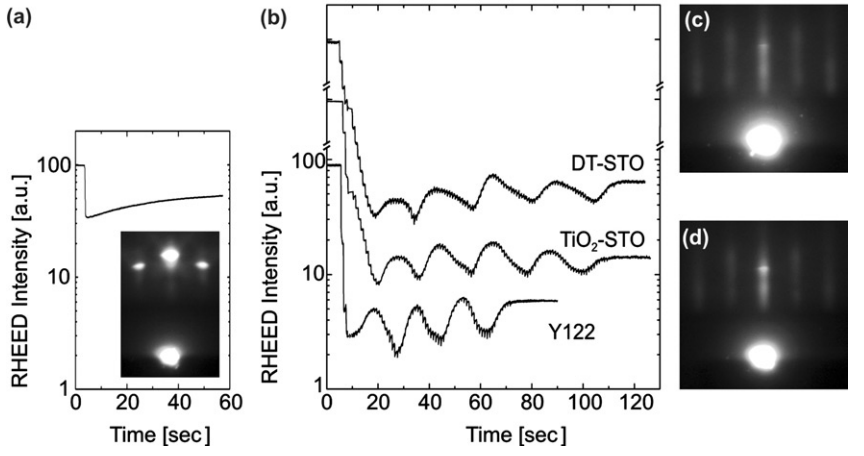

Figure 3. RHEED intensity recorded during growth of Y123 ultrathin films with different control on the interface stacking. (a) Deposition of the initial Y122 layer on TiO_2-terminated STO. (b) Deposition of Y123 on DT and single (TiO_2)-terminated STO and on the Y122 layer.
Notes: The RHEED patterns are shown after (inset in a) the initial Y122 layer, (c) and (d) the deposition of Y123 on DT-STO and Y122, respectively.

RHEED intensity was observed during growth of the initial Y122 layer see Figure 3(a). This and the corresponding RHEED pattern, exhibiting clear two-dimensional spots see inset Figure 3(a), indicated a perfect and atomically flat crystalline surface. During subsequent deposition of Y123, clear intensity oscillations are observed, which indicated 2D growth, see Figure 3(b). Oscillations of the specular RHEED intensity were also observed during deposition of Y123 on double terminated (DT) and TiO_2-terminated STO substrates, but the recovery was smaller than in the case of an initial Y122 layer. Moreover, on a DT-STO substrate only streaks could be seen (Figure 3c), while clear 2D spots were observed in the RHEED pattern of Y123 on Y122 (Figure 3d). Both facts reflected that the surface step density and, therefore, the surface roughness increased when increasing the number of possible interface stacking sequences.

In order to analyze the in-plane ordering and, subsequently, the network of antiphase boundaries, the (00*l*)-rocking curves (ω-scans) were measured by X-ray diffraction (XRD). In Figure 4(a), (005)-rocking curves are shown for 10 u.c. of Y123 grown on an initial Y122 layer and on DT-STO. In both cases, the observed shape exhibits two parts: a satellite (broad) component and a main peak (narrow component), which is characteristic for weakly disordered systems [19]. The coherent peak, related to perfectly aligned regions, cannot be resolved due to the resolution limitation of the apparatus. The line shapes of the broad components are different in both cases (Gaussian on an initial Y122 layer and Lorentzian on DT-STO), which has been previously attributed to different densities of APBs [20]. Moreover, on increasing the number of possible interfacial configurations, the ratio between the intensity of the narrow and broad components (R) decreases from $R=3$ for Y123 grown on an initial Y122 layer to $R=2$ for Y123 grown on DT-STO. This is caused by the extension of the diffuse spots perpendicularly to the diffraction vector when increasing the defect density [19]. Further information on the disorder as a function of interface engineering can be obtained by comparing the co-scans of different (00*l*)-reflections. Lattice mismatched epitaxial layers such as the Y123 films can be considered as separated mosaic blocks on a substrate. In this picture, the diffuse

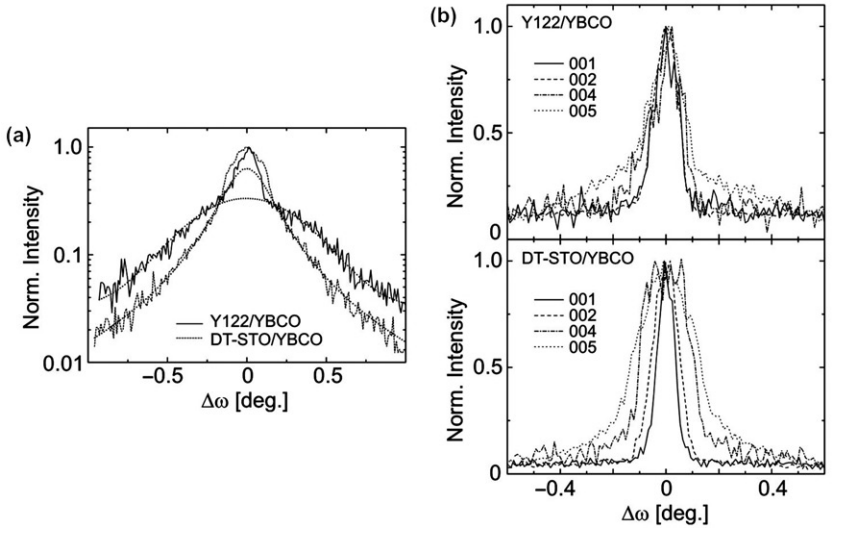

Figure 4. Normalized (00*l*)-rocking curves of Y123 films (10 u.c.) with different SSI with the substrate. (a) The (005)-rocking curves of Y123 films grown on Y122 and DT-STO, presenting the two component characteristics of weakly disordered systems. (b) The (00*l*)-rocking curves ($l = 1, 2, 4, 5$) of Y123 grown on Y122 and DT-STO, showing, respectively, a constant and an increasing angular width.

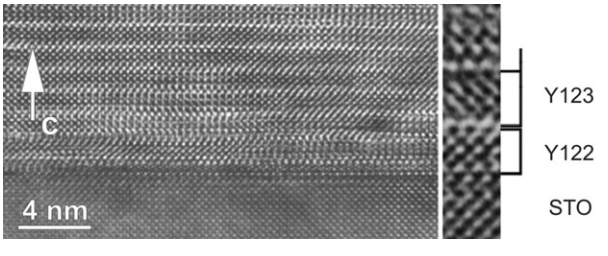

Figure 5. HREM image of an Y123 film with a single u.c. of Y122 as buffer layer on a TiO_2-terminated STO substrate.
Note: An enlargement of the film-substrate interface is also shown.

component of the rocking curve is influenced by two main factors: slightly in-plane misorientation and small coherence length parallel to the substrate [21]. In Figure 4(b) it is shown that the main peak of Y123 with an initial Y122 layer presents a constant lateral width in angle space, $\Delta w = w - q_1$, with q_1 being the position of the corresponding Bragg reflection, which is a clear indication of disorder of rotational nature [20]. Meanwhile, the film on DT-STO exhibits a width increase with l, which means that the broadening of the rocking curve is related also to a shortening of the coherence length caused by a higher density of in-plane defects.

All these observations are supported by HREM analysis of a pulsed laser deposited Y123 film grown on TiO_2-terminated STO with a Y122 single unit cell buffer layer, see Figure 5. It proves that using an initial Y122 layer results in a high-quality film with good epitaxial properties: $(001)_{Y123}$ parallel to $(001)_{STO}$ and $(100)_{Y123}$ parallel to $(100)_{STO}$ [22,23]. The misfit between film and substrate (~2%) causes local bending of the lattice planes. Antiphase boundaries in the film occur only occasionally and their spacing

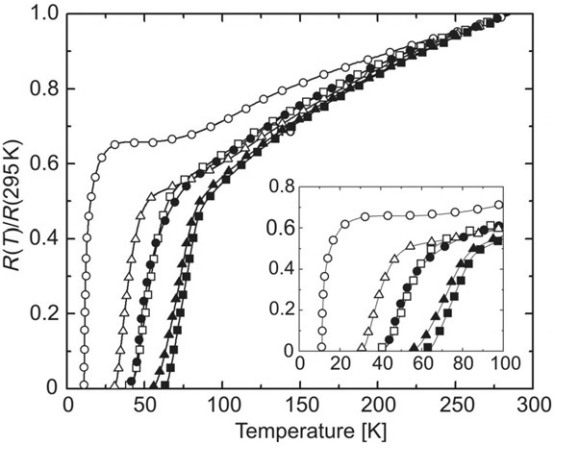

Figure 6. Temperature dependence of the normalized resistance curves for 7-unit-cell-thick films with different degrees of control at the interface.
Note: Y122 (open circle), TiO_2–STO (open triangle) and DT-STO (open square). The closed symbols mark the normalized resistance after a post-growth oxidation treatment.

is comparable with the terrace width. Therefore, it can be concluded that antiphase boundaries are only formed at unit cell steps at the substrate surface and not as a result of a variable interface configuration. Consequently, the interface stacking sequence of this film is the single type as shown in Figure 2(c).

In Figure 6, the normalized electrical resistance against temperature curves are given for 7-unit-cell-thick films with the three available interface configurations. It can be seen that there is a close relationship between the electrical properties and the density of APBs, controlled by the number of SSIs. It is shown that a higher density of APBs leads to a higher superconducting transition temperature, T_c, and a steeper slope of the temperature dependence of the normal state resistance. This behaviour is attributed to the degree of oxidation of the YBCO ultrathin films, since these planar defects are supposed to favour oxygen in-diffusion in Y123 thin films, in a similar way as other defects, like dislocations, do [24]. Oxygen diffusion in the *c*-direction in a single crystal, without any defects, is 10^4-10^6 times slower than diffusion in the (a, b)-direction [25,26]. An observation giving support to this idea is that after a post-growth oxidation treatment of these films in 1 bar oxygen at 600°C for 6 h and 450°C for 18 h, T_c tends to approach the same value for all ultrathin films, as shown in the inset in Figure 6. This indicates that the low concentration of defects in the film with the Y122 interface is the main cause for the oxygen deficiency and, therefore, the reduced superconducting properties observed in these as-made films. The diffusion of oxygen in the film is comparatively slower and requires longer oxidation times. In other words, the presence of APBs in the thin films favours the oxygen in-diffusion, but is unfortunately accompanied by an increase in the disorder [27].

3.1. *Strain relaxation in ultrathin films*

Heteroepitaxial growth of thin films can produce strained heterostructures in the case of low misfit substrates. If the lattice mismatch between substrate and growing epitaxial layer is sufficiently small, the first deposited atomic layers will be strained to match the substrate, until a critical thickness is reached, above which relaxation takes place by

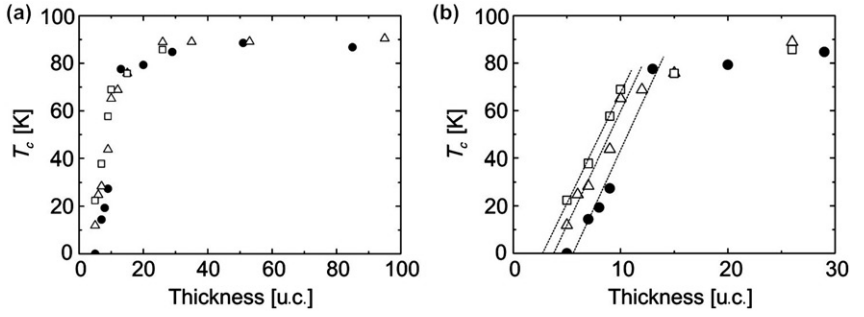

Figure 7. The transition temperature T_c ($R=0$) as a function of the thickness of the YBCO layer for different degrees of control at the substrate interface. (a) All films have comparable T_c values (~90 K) for large thickness, (b) but show different behaviour for ultrathin films (below ~15 u.c.). Notes: Y122 (closed circle), TiO_2–STO (open triangle) and DT-STO (open square). The dashed lines indicate the increase in T_c with thickness for ultrathin films.

introduction of twins and/or dislocations. Y123 thin films are grown at high temperatures where the equilibrium phase is tetragonal, but they undergo a phase transition to orthorhombic upon cooling. The relaxation of these films has to accommodate not only a lattice mismatch, but also this tetragonal-orthorhombic transition. Several strain relieving mechanisms have been proposed for Y123 deposited on STO by PLD with critical thicknesses ranging between 5 and 20 nm, ~4 and 17 u.c. [18,28–31]. The large difference in the experimentally determined critical thickness values was supposed to be a result of the different growth conditions. These growth conditions determine the surface morphology and therefore the nucleation of dislocations.

Strain relaxation in a structurally perfect film with a smooth surface is very difficult. In case of Y123, growth dislocations are formed to reduce the epitaxial strain, only after a critical thickness for an initial pseudomorphic layer. The critical thickness was indeed found to be dependent on the surface termination of the STO substrate [17] with the highest critical thickness for TiO_2 terminations. It has also been observed that the epitaxial relationship between the film and the substrate is influenced by the magnitude of the miscut angle of the vicinal (001) STO substrates. Up to a miscut angle of 1.2°, Y123 films grow on the optical surface, whereas above this angle films are grown on the crystallographic surface [32–34]. The reported critical thickness for Y123 grown on TiO_2-terminated STO substrates by PLD, corresponding to the point of tetragonal to orthorhombic transition, is ~11.5 nm for low miscut angles [35].

To investigate the influence of the density of APB's on the strain relaxation, Y123 layers with different thicknesses were grown on Y122, TiO_2–STO and DT-STO. The deposition conditions are described in the experimental section. During deposition of Y123, clear intensity oscillations were observed up to a thickness of~20 u.c, which was used to determine the exact layer thickness. For thicker films the total thickness was estimated from the growth rate at the initial stage. Figure 7(a) shows the variation in transition temperature T_c ($R=0$) with the number of YBCO unit cells for different densities of APB's at the STO substrate. The control of the APB density, enabled by growth on Y122, TiO_2–STO and DT-STO, will influence the formation of dislocations and therefore, the strain relaxation. For thicker films, the effect of the initial APB density on the transition temperature is negligible and the T_c is ~90 K. However, the APB density does play an important role for ultrathin films below ~15 u.c., see Figure 7(b). Y123 layers with a thickness of 5 unit cells do not become superconducting when grown on an Y122

layer, due to the low number of APB's and the corresponding low level of oxygen in-diffusion. On the other hand, when 5-unit-cell-thick YBCO is grown on TiO_2-terminated STO and DT-STO, the density of APB's increases and causes better oxidation of the film. This leads to superconductivity with T_c values of 11.9 and 22.4 K for Y123 films on respectively, TiO_2–STO and DT-STO.

By increasing the thickness of the Y123 layer, the number of dislocations to release the strain increases, which improves the oxygen in-diffusion. This will induce an increase in the transition temperature, which is visible in Figure 7(b) for all three cases of substrate terminations. For all three, the increase in T_c with every extra Y123 layer is comparable and is about 9.6 K per u.c. This means that although the density of APBs at the beginning of the growth is different, the formation of dislocations to release the strain is similar during subsequent growth. This results in different thickness values for the transition from non-superconductivity to superconductivity. Critical thickness were estimated from linear fits to be: 5.2 u.c. (6.1 nm), 3.4 u.c. (4.0 nm) and 2.4 u.c. (2.8 nm) for Y123 layers on, respectively, Y122, TiO_2–STO and DT-STO. The thickness where the strain appears to be relaxed for the major part of the film, and only a small increase in T_c is visible for higher values, is different for the three cases. The Y123 layer on DT-STO seems to be relaxed after ~10 u.c., while this thickness value is slightly higher in case of growth on single-terminated TiO_2–STO, namely ~11 u.c. The major part of the Y123 layer grown on the Y122 layer appears to be relaxed after ~13 u.c. These values agree very well with results from other groups for pulsed laser deposited Y123 on STO, but show clearly the dependence of the critical thickness on the initial defect (APB) density at the film-substrate interface.

Due to the substrate-induced strain, ultrathin films will have in-plane lattice parameters comparable to those of the substrate. This leads to the pseudomorphic Y123 phase with in-plane tensile strain and, therefore, out-of-plane shortening of the *c*-axis. To study the relationship between the thickness of the Y123 layer and the substrate-induced strain, the films were examined by XRD. The θ–2θ scans along the direction normal to the surface exhibit only (00*l*) reflections, which implies that the films are *c*-axis oriented, see Figure 8. No other peaks are observed indicating the absence of unwanted phases. Y123 films grown on STO with an initial Y122 layer are shown for total thicknesses of 9, 15 and 40 u.c. The observation of the (00*l*) reflections allows calculation of the *c*-axis lattice parameter by using Bragg's law. This is an advantage, because determination of the unit cell structure by fitting of numerous peaks is not possible for ultrathin films, as only the (00*l*) reflections are sufficiently strong to be observed. The value for the *c*-axis can be calculated by comparing the Bragg angles of the (005) Y123 peak and the (002) STO peak:

$$C_{Y123} = a_{STO} \frac{N_{Y123}}{N_{STO}} \frac{\sin\theta_{STO}}{\sin\theta_{Y123}}$$

where $a_{STO} = 3.905$ Å is the lattice constant of the cubic STO substrate and θ_{STO} and θ_{Y123} are the Bragg angles of the STO and Y123 peaks. N_{STO} and N_{Y123} indicate the reflection orders of the STO and Y123 reflection peaks. The calculated *c*-axis lattice parameters are given in Figure 9 for Y123 layers with different thickness on STO with an initial Y122 layer as well as on DT-STO and TiO_2-terminated STO. The Y123 films show a decrease in *c*-axis length for all three cases when the thickness is decreased. Below a critical thickness, a reduced *c*-axis is expected due to a contraction of the *c*-axis caused by the in-plane tensile strain from the larger substrate lattice. The Y123 films on DT-and TiO_2–STO show this

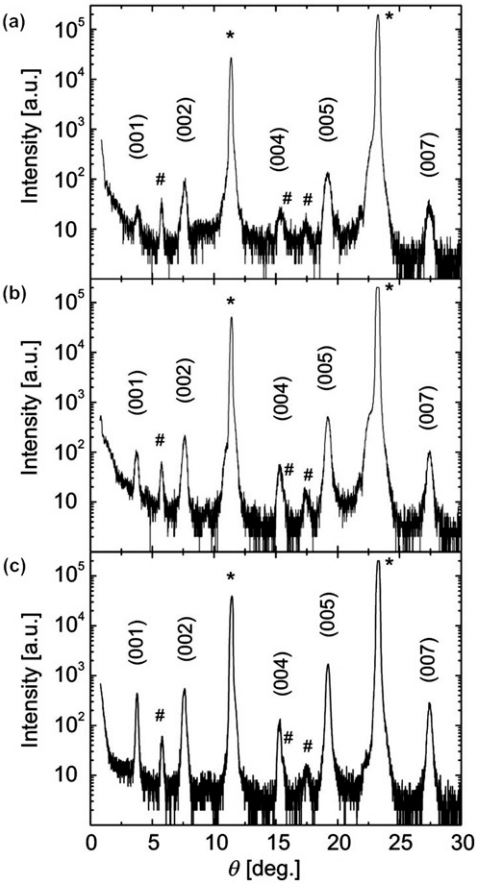

Figure 8. XRD θ–2θ scans of Y123 layers on TiO_2-terminated $SrTiO_3$ with an Y122 initial layer.
Notes: The thickness of the total YBCO layer is (a) 9, (b) 15 and (c) 40 u.c. The $SrTiO_3$ substrate reflections are indicated with an asterisk and their spectral contributions ($\lambda/2$ and $\lambda/3$) with a cross.

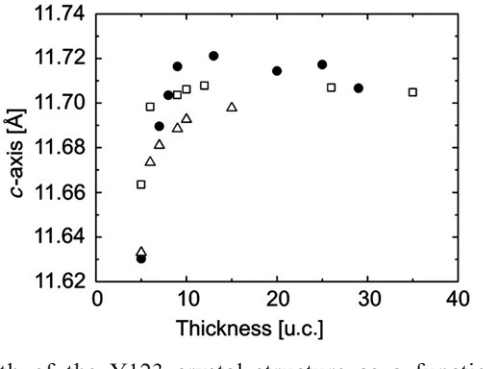

Figure 9. The *c*-axis length of the Y123 crystal structure as a function of the layer thickness for different degrees of control at the substrate interface.
Note: Y122 (open circle), TiO_2–STO (open triangle) and DT-STO (open square).

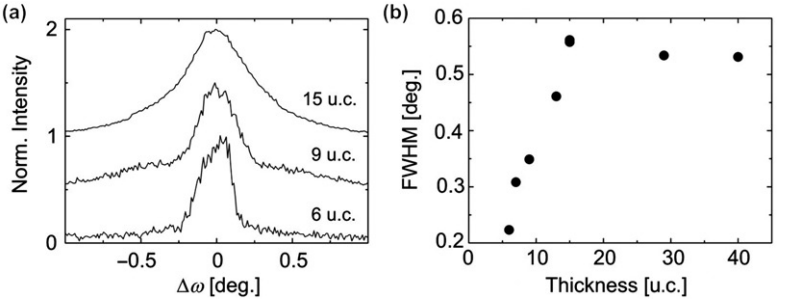

Figure 10. Thickness dependence of the (005)-rocking curve of Y123 grown on TiO_2-terminated STO with an initial Y122 layer. (a) Normalized X-ray (005)-rocking curves of 6, 9 and 15 u.c. thick Y123 films. For clarity are the curves of the 9 and 15 u.c. thick Y123 films displaced by respectively, 0.5 and 1.0. (b) Thickness dependence of the FWHM of the (005) Y123 rocking curves.

decrease in *c*-axis below 10–12 u.c. Surprisingly, the Y123 films on the initial Y122 layer show a small increase in *c*-axis when the thickness is decreased to ~12 u.c., followed by a sharp drop in *c*-axis when the thickness is further reduced. This is caused by the interplay of two mechanisms, strain relaxation and oxygenation, which have opposite effects on the *c*-axis parameter. While for ultrathin films with a low defect density the *c*-axis is reduced due to large in-plane tensile strain, at the same time this highly-ordered structure leads to a low level of oxygen incorporation, which results in an enlargement of the *c*-axis. The observation of a reduced *c*-axis for ultrathin films is in good agreement with results for sputter deposition [36,37], but contradict earlier results by pulsed laser deposition [20]. An important point is the $SrRuO_3$ cap layer in these experiments, which was not present in the other PLD experiments. This cap layer will protect the delicate ultrathin films and prevent the exposure to ambient atmosphere, which can affect the surface and degrade the superconducting layer. The relaxation of the in-plane lattice parameters could not be verified, as only the (00*l*) reflections in the ultrathin films are sufficiently strong to be observed. However, (00*l*)-rocking curves provide important information on the lattice perfection of the thin films. Rocking curves (ω-scans) were taken around the (005) reflection of the Y123 layer on the initial Y122 layer. The rocking curves initially exhibit a broad and a narrow component, see Figure 10(a). The narrow peak indicates that the lattice is highly ordered and in a strained pseudomorphic status. The peak broadening, which can be observed for an increase in thickness, can be attributed to the increase of the number of defects by the strain relaxation. The values for the full width at half maximum (FWHM) are given in Figure 10(b). They show an increase up to a thickness of ~15 u.c., after which the FWHM value becomes constant at ~0.55°. This value is in good agreement with results for thick pulsed laser deposited Y123 films from other groups [20,38]. These findings strongly imply that the defect density depends on the thickness. When the layer thickness reaches the critical value at ~15 u.c., the major part of the strain is relieved and the defect density stays constant for thicker films.

4. Conclusions

Here, we have shown a clear example where the structural properties and surface morphology of a thin film material are a direct result of thin film growth, influenced by deposition conditions and substrate properties. Most importantly, the atomic stacking sequence at the substrate-film interface plays an essential role in the heteroepitaxial growth

of Y123. During initial growth, the interface configuration influences the surface morphology and structural properties of the film, due to the formation of anti-phase boundaries by coalescence of islands with different stacking sequences. The interface configuration can be accurately controlled by both the terminating atomic layer of the STO substrate and the stoichiometry of the first unit cell layer. Using this capability, the network of anti-phase boundaries and therefore, the in-plane ordering is tuned, as well as its influence on the structural and electrical properties of the Y123 film. The superconducting transition temperature was found to be depressed by improvement of the in-plane ordering, which strongly indicates that the absence of anti-phase boundaries hampers the oxygen in-diffusion. We demonstrated that in the heteroepitaxial growth of Y123 on STO the first deposited atomic layers are strained to match the substrate, due to the small lattice mismatch. However, above a critical thickness for this strained pseudomorphic layer the strain will relax by the introduction of defects. The initial defect density, which is already present at the substrate-film interface, will determine the value for this critical thickness during subsequent growth, because the process of strain relaxation is improved by the number of antiphase boundaries.

Acknowledgements

Part of the presented research was performed by the late S.R. Currás. This work is part of the research program of the Foundation for Fundamental Research on Matter (FOM, financially supported by the Netherlands Organization for Scientific Research (NWO)). G. Koster, D.H.A. Blank and G. Rijnders acknowledge additional support from NWO.

References

[1] R.J. Cava, R.B. Van Dover, B. Batlogg, and E.A. Rietman, *Bulk superconductivity at 36 K in* $La_{1.8}Sr_{0.2}CuO_4$, Phys. Rev. Lett. 58 (1987), pp. 408–410.

[2] C.W. Chu, P.H. Hor, R.L. Meng, L. Gao, Z.J. Huang, and Y.Q. Wang, *Evidence for superconductivity above 40 K in the La–Ba–Cu–O compound system*, Phys. Rev. Lett. 58 (1987), pp. 405–407.

[3] ———, *Superconductivity at 52.5 K in the Lanthanum–Barium–Copper–Oxide system*, Science 235 (1987), pp. 567–569.

[4] M.K. Wu, J.R. Ashburn, C.J. Torng, P.H. Hor, R.L. Meng, L. Gao, Z.J. Huang, Y.Q. Wang, and C.W. Chu, *Superconductivity at 93 K in a new mixed-phase Y–Ba–Cu–O compound system at ambient pressure*, Phys. Rev. Lett. 58 (1987), pp. 908–910.

[5] R.J. Cava, B. Batlogg, R.B. Van Dover, D.W. Murphy, S. Sunshine, T. Siegrist, J.P. Remeika, E.A. Rietman, S. Zahurak, and G.P. Espinosa, *Bulk superconductivity at 91 K in single-phase oxygen-deficient perovskite* $Ba_2YCu_3O_{9-\delta}$, Phys. Rev. Lett. 58 (1987), pp. 1676–1679.

[6] J.D. Jorgensen, M.A. Beno, D.G. Hinks, L. Soderholm, K.J. Volin, R.L. Hitterman, J.D. Grace, I.K. Schuller, C.U. Segre, K. Zhang et al., *Oxygen ordering and the orthorhombic-to-tetragonal phase transition in* $YBa_2Cu_3O_{7-x}$, Phys. Rev. B 36 (1987), pp. 3608–3616.

[7] A.J.H.M. Rijnders, *The initial growth of complex oxides: study and manipulation, Chapter 5,* Ph.D. thesis, University of Twente, The Netherlands, 2001.

[8] T. Terashima, Y. Bando, K. Iijima, K. Yamamoto, K. Hirata, K. Hayashi, K. Kamigaki, and H. Terauchi, *Reflection high-energy electron diffraction oscillations during epitaxial growth of high-temperature superconducting oxides*, Phys. Rev. Lett. 65 (1990), pp. 2684–2687.

[9] H. Karl and B. Stritzker, *Reflection high-energy electron diffraction oscillations modulated by laser-pulse deposited* $YBa_2Cu_3O_{7-x}$, Phys. Rev. Lett. 69 (1992), pp. 2939–2942.

[10] J.M. Phillips, *Substrate selection for high-temperature superconducting thin films*, J. Appl. Phys. 79 (1996), pp. 1829–1848.
[11] G. Koster, B.L. Kropman, G.J.H.M. Rijnders, D.H.A. Blank, and H. Rogalla, *Quasi-ideal strontium titanate crystal surfaces through formation of strontium hydroxide*, Appl. Phys. Lett. 73 (1998), pp. 2920–2922.
[12] G. Koster, G.J.H.M. Rijnders, D.H.A. Blank, and H. Rogalla, *Imposed layer-by-layer growth by pulsed laser interval deposition*, Appl. Phys. Lett. 74 (1999), pp. 3729–3731.
[13] S. Bals, G. Rijnders, D.H.A. Blank, and G. Van Tendeloo, *TEM of ultra-thin $DyBa_2Cu_3O_{7-x}$ films deposited on TiO_2 terminated $SrTiO_3$*, Physica C 355 (2001), pp. 225–230.
[14] J.G. Wen, C. Traeholt, and H.W. Zandbergen, *Stacking sequence of $YBa_2Cu_3O_7$ thin film on $SrTiO_3$ substrate*, Physica C 205 (1993), pp. 354–362.
[15] B. Dam, C. Træholt, B. Stäuble-Pümpin, J. Rector, and D.G. De Groot, *The relation between the defect structure, the surface roughness and the growth conditions of $YBa_2Cu_3O_{7-\delta}$ films*, J. Alloys Compd. 251 (1997), pp. 27–30.
[16] J. Zegenhagen, T. Siegrist, E. Fontes, L.E. Berman, and J.R. Patel, *Epitaxy of ultrathin films of $YBa_2Cu_3O_{7-\delta}$ on $SrTiO_3(001)$ investigated with X-ray standing waves*, Solid State Comm. 93 (1995), pp. 763–767.
[17] J.M. Huijbregtse, J.H. Rector, and B. Dam, *Effect of the two (100) $SrTiO_3$ substrate terminations on the nucleation and growth of $YBa_2Cu_3O_{7-\delta}$ thin films*, Physica C 351 (2001), pp. 183–199.
[18] X.-Y. Zheng, D.H. Lowndes, S. Zhu, J.D. Budai, and R.J. Warmack, *Early stages of $YBa_2Cu_3O_{7-\delta}$ epitaxial growth on MgO and $SrTiO_3$*, Phys. Rev. B 45 (1992), pp. 7584–7587.
[19] V.M. Kaganer, R. Köhler, M. Schmidbauer, R. Opitz, and B. Jenichen, *X-ray diffraction peaks due to misfit dislocations in heteroepitaxial structures*, Phys. Rev. B 55 (1997), pp. 1793–1810.
[20] B. Dam, J.M. Huijbregtse, and J.H. Rector, *Strong pinning linear defects formed at the coherent growth transition of pulsed-laser-deposited $YBa_2Cu_3O_{7-\delta}$ films*, Phys. Rev. B 65 (2002), p. 064528.
[21] P.F. Miceli and C.J. Palstrom, *X-ray scattering from rotational disorder in epitaxial films: an unconventional mosaic crystal*, Phys. Rev. B 51 (1995), pp. 5506–5509.
[22] S. Bals, *Optimisation of superconducting thin films and tapes by transmission electron microscopy, Chapter 4*, Ph.D. thesis, University of Antwerp, Belgium, 2003.
[23] S. Bals, G. Van Tendeloo, G. Rijnders, M. Huijben, V. Leca, and D.H.A. Blank, *Transmission electron microscopy on interface engineered superconducting thin films*, IEEE Trans. Appl. Supercond. 13 (2003), pp. 2834–2837.
[24] A. Kursumovic, P. Berghuis, V. Dediu, J.E. Evetts, F.C. Matacotta, and G.A. Wagner, *Thickness-dependent oxygenation in c-axis oriented $ReBa_2Cu_3O_{7-\delta}$ thin films deposited on closely matched substrates*, Physica C 331 (2000), pp. 185–190.
[25] K.N. Tu, N.C. Yeh, S.I. Park, and C.C. Tsuei, *Diffusion of oxygen in superconducting $YBa_2Cu_3O_{7-\delta}$ ceramic oxides*, Phys. Rev. B 39 (1989), pp. 304–314.
[26] S.J. Rothman, J.L. Routbort, U. Welp, and J.E. Baker, *Anisotropy of oxygen tracer diffusion in single-crystal $YBa_2Cu_3O_{7-\delta}$*, Phys. Rev. B 44 (1991), pp. 2326–2333.
[27] G. Rijnders, S. Curras, M. Huijben, D.H.A. Blank, and H. Rogalla, *Influence of substrate-film interface engineering on the superconducting properties of $YBa_2Cu_3O_{7-\delta}$*, Appl. Phys. Lett. 84 (2004), pp. 1150–1152.
[28] T.-S. Gau, S.-L. Chang, H.-H. Hung, C.-H. Lee, T.-W. Huang, H.-B. Lu, S.-J. Yang, and S.-E. Hsu, *Direct observation of the interface structure of thin $YBa_2Cu_3O_x$ film (<500 Å) deposited on $SrTiO_3(001)$ utilizing grazing incidence X-ray diffraction*, Appl. Phys. Lett. 65 (1994), pp. 1720–1722.
[29] T. Frey, C.C. Chi, C.C. Tsuei, T. Shaw, and F. Bozso, *Effect of atomic oxygen on the initial growth in thin epitaxial cuprate films*, Phys. Rev. B 49 (1994), pp. 3483–3491.
[30] A. Abert, J.P. Contour, A. Défossez, D. Ravelosona, W. Schwegle, and P. Ziemann, *Critical thickness of YBaCuO (123) strained thin films and superlattices grown by pulsed laser deposition*, Appl. Surf. Science 96 (1996), pp. 703–707.
[31] L.X. Cao, J. Zegenhagen, E. Sozontov, and M. Cardona, *The effect of epitaxial strain on $RBa_2Cu_3O_7$ thin films and the perovskite substrate*, Physica C 337 (2000), pp. 24–30.

[32] J.M. Dekkers, G. Rijnders, S. Harkema, H.J.H. Smilde, H. Hilgenkamp, H. Rogalla, and D.H.A. Blank, *Monocrystalline $YBa_2Cu_3O_{7-\delta}$ thin films on vicinal $SrTiO_3(001)$ substrates*, Appl. Phys. Lett. 83 (2003), pp. 5199–5201.

[33] J.L. Maurice, O. Durand, M. Drouet, and J.-P. Contour, *Microstructure and strain relaxation in $YBa_2Cu_3O_7$ epitaxial thin films*, Thin Solid Films 319 (1998), pp. 211–214.

[34] L. Mechin, P. Berghuis, and J.E. Evetts, *Properties of $YBa_2Cu_3O_{7-\delta}$ thin films grown on vicinal $SrTiO_3(001)$ substrates*, Physica C 302 (1998), pp. 102–112.

[35] V. Vonk, S.J. VanReeuwijk, J.M. Dekkers, S. Harkema, A.J.H.M. Rijnders, and H. Graafsma, *Strain-induced structural changes in thin $YBa_2Cu_3O_{7-x}$ films on $SrTiO_3$ substrates*, Thin Solid Films 449 (2004), pp. 133–137.

[36] H.Y. Zhai and W.K. Chu, *Effect of interfacial strain on critical temperature of $YBa_2Cu_3O_{7-\delta}$ thin films*, Appl. Phys. Lett. 76 (2000), pp. 3469–3471.

[37] M. Varela, W. Grogger, D. Arias, Z. Sefrioui, C. Léon, L. Vazquez, C. Ballesteros, K.M. Krishnan, and J. Santamaria, *Effects of epitaxial strain on the growth mechanism in $YBa_2Cu_3O_{7-x}$ thin films in $YBa_2Cu_3O_{7-x}/PrBa_2Cu_3O_7$ superlattices*, Phys. Rev. B 66 (2002), p. 174514.

[38] J.D. Pedarnig, R. Rössler, M.P. Delamare, W. Lang, D. Bäuerle, A. Köhler, and H.W. Zandbergen, *Electrical properties, texture, and microstructure of vicinal $YBa_2Cu_3O_{7-\delta}$ thin films*, Appl. Phys. Lett. 81 (2002), pp. 2587–2589.